 doi:10.20944/preprints202109.0444.v1

Article

Bidirectional Electric-induced Conductance based on GeTe/Sb_2Te_3 Interfacial Phase Change Memory for Neuro-inspired Computing

Shin-young Kang [1], Soo-min Jin [3], Ju-young Lee [3], Dae-seong Woo [3], Tae-hun Shim [4], In-ho Nam [5], Jea-gun Park [3,4,5], Yuji Sutou[1,2] and Yun-heub Song [3,4,*]

[1] Department of Materials Science, Tohoku University, Sendai, Japan; kang.shinyoung.p4@dc.tohoku.ac.jp
[2] WPI Advanced Institute for Materials Research, Tohoku University, Sendai, Japan;
[3] Department of Nano-scale Semiconductor Engineering, Hanyang University, Seoul, Republic of Korea;
[4] Advanced Semiconductor Materials and Devices Development Center, Hanyang University, Seoul, Republic of Korea;
[5] Department of Electronics Engineering, Hanyang University, Seoul, Republic of Korea;
* Correspondence: yhsong2008@hanyang.ac.kr; Tel.: +82-2-2220-4136

Abstract: Corresponding to the principles of biological synapses, an essential prerequisite for hardware neural networks using electronics devices is continuous regulation of conductance. We implemented artificial synaptic characteristics in a $(GeTe/Sb_2Te_3)_{16}$ iPCM with a superlattice structure under optimized identical pulse trains. Based on atomically controlling the Ge switch in the phase transition that appears in the $GeTe/Sb_2Te_3$ superlattice structure, multiple conductance states were implemented by applying the appropriate electrical pulses. Furthermore, we found that the bidirectional switching behavior of a $(GeTe/Sb_2Te_3)_{16}$ iPCM can achieve a desired resistance level using the pulse width. Therefore, we also fabricated a $Ge_2Sb_2Te_5$ PCM and designed a pulse scheme based on the phase transition mechanism to compare to the $(GeTe/Sb_2Te_3)_{16}$ iPCM. We designed an identical pulse scheme that implements linear and symmetrical LTP and LTD based on the iPCM mechanism. As a result, the $(GeTe/Sb_2Te_3)_{16}$ iPCM showed relatively excellent synaptic characteristics by implementing gradual conductance modulation, a nonlinearity value of 0.32, and LTP/LTD 40 conductance states using identical pulses trains. Our results demonstrate the general applicability of the artificial synaptic device for potential use in neuro-inspired computing and next generation non-volatile memory.

Keywords: interfacial phase change memory; phase change memory; artificial synaptic device; superlattice; neuromorphic devices;

1. Introduction

As artificial intelligence (AI) technologies have generated considerable recent research interest, technological advancements for handling large amounts of data are increasingly necessary [1-3]. In the big data era, conventional computational systems based on von Neumann architecture are limited in their ability to efficiently transfer data between memory and computing units due to a bottleneck [4]. In the past few decades, neuro-inspired computing has made remarkable progress in achieving human brain-like performance using electronic devices that can implement adaptive parallel processing [1]. Such systems have been executed in the field of hardware neural networks (HW-NNs) that consist of numerous artificial synapses that perform cognitive and computational capabilities. Numerous experiments have successfully emulated several characteristics of biological synapses, such as updating or memorizing (called a synaptic weight) the conductance of electronic devices using an external voltage or optical stimulus [5,6]. One of the most promising hardware platforms used for implementing an artificial synapse is emerging non-volatile memory (eNVM) devices, which have extremely compact designs

Preprints (www.preprints.org) | NOT PEER-REVIEWED | Posted: 27 September 2021 doi:10.20944/preprints202109.0444.v1

using a two-terminal structure. Categories of eNVM include resistive random-access memory (RRAM) [7], ferromagnetic random-access memory, (FeRAM) [8], and phase change random-access memory (PCRAM) [9] according to the physical mechanism used in each. Despite the progress that has been made in eNVM devices, there are still many challenges to overcome before they can achieve the same level of accuracy as the biological brain and software neural networks [2]. These challenges arise from eNVM operation that does not sufficiently satisfy the required synaptic characteristics, such as linear/symmetric conductance change, device-to-device variation, dynamic range, and the number of conductance states.

Among the various eNVMs, $Ge_2Sb_2Te_5$ (GST225), one of the representative materials of PCRAM, is a 2-terminal device that has been heavily researched regarding synaptic device applications [10]. It operates by differentiating the resistance between the crystalline state of the phase change material with high electrical conductivity from the metastable amorphous states with low electrical conductivity. Switching is generally performed by Joule heating of the amorphous material to above the crystalline temperature of 150 °C to create the conductive state. Conversely, the highly resistive amorphous state is achieved by melting the crystalline material above 625 °C and subsequent quenching [11]. Based on this melting-quenching mechanism, the change in analog conductance for neuro-inspired computing in phase change materials can be classified according to the volume ratio of the crystalline to the amorphous states [2,9]. Due to these characteristics, GST225 is well known to have advantages in scalability, reliability, and multi-level resistance programming. However, operating GST225 with Joule heating consumes a lot of energy as rapid high-current pulses must be applied to achieve the amorphous state [11]. In addition, it is difficult to precisely control the phase change volume to implement gradual conductance state changes and long-term potentiation (LTP) and long-term depression (LTD), which are used to emulating synaptic weight [9]. Although this issue can be overcome through the 2-PCM architecture and peripheral circuit design, there are still limitations with respect to complex device operation and scalability [12].

To address these issues, interfacial phase change memory (iPCM) based on van der Waals heterostructures have been developed by alternately depositing ultra-thin films of $(GeTe/Sb_2Te_3)n$, where n is the number of stacked layers, as proposed by Tominaga *et al* [13]. The iPCM superlattice structure is designed such that the Ge atoms in the GeTe layers undergo vertical and lateral displacement at the thin film surface. Although the specific mechanism of the iPCM operation has not been definitively established, it is clear that when an external voltage is applied to the iPCM, the Ge atoms play a key role by changing the bonding structure between high resistance covalent bonding and low resistance resonant bonding [14,15]. Therefore, the iPCM reduces the total entropy by limiting the movement of Ge atoms by establishing a vdW gap between the thin films [13]. This process enables the iPCM to consume less energy than GST225 and achieve faster device operation. Furthermore, it is highly probable that iPCMs provide more sophisticated resistance changes in restraining atomic movement, which maintains the crystalline states. However, there remains a need to effectively demonstrate synaptic properties exploited in neuro-inspired computing by changing conductance values.

In this study, to understand the application of HH-NNs, we fabricated sputter-grown iPCMs based on the $GeTe/Sb_2Te_3$ superlattice structure. We further examined the dependence of conductance on the voltage-based electrical pulse width by analyzing bidirectional of the $(GeTe/Sb_2Te_3)_{16}$ iPCM by applying incremental step pulse programming. Based on this relationship, an optimized sequence of identical fast pulses was designed and applied to the $(GeTe/Sb_2Te_3)_{16}$ iPCM to implement linear and gradual conductance modulation. We present the possibility of utilizing artificial synapses through a newly designed iPCM device with a superlattice structure.

2. Experimental Procedures

All thin films used in the iPCM samples were fabricated with a multi-chamber cluster sputtering system without vacuum breaking under a high vacuum of $< 1 \times 10^{-8}$ torr. Com-

Preprints (www.preprints.org) | NOT PEER-REVIEWED | Posted: 27 September 2021 doi:10.20944/preprints202109.0444.v1

posite GeTe and Sb_2Te_3 targets were acquired by alternately opening and closing respective shutters for growth of the superlattice structures. To determine the effect of growth temperature, a two-step growth method was applied under various annealing temperatures, which is known to be extremely effective for fabrication of highly oriented iPCMs [16]. As shown in the schematic of an iPCM sample in Figure 1a, an amorphous seed layer of Sb_2Te_3 with a thickness of 5 nm is deposited at room temperature on TiN, which acts as a bottom electrode contact (BEC). The Sb_2Te_3 serves as a template that determines the orientation of the atomic arrangement of subsequently deposited thin films. Next, annealing is carried out at 210 °C to 270 °C while the seed layer is deposited. While maintaining the annealing temperature, 1 nm of GeTe and 4 nm of Sb_2Te_3 were alternately deposited 16 times to obtain a superlattice of 80 nm thickness in total. Finally, after depositing 50 nm of TiN as the top electrode contact (TEC), patterning and ion milling is performed to complete the fabrication.

We used the Cu-Kα radiation X-ray diffraction (XRD) to evaluate the orientation of the iPCM samples synthesized with different annealing temperatures. High-resolution transmission electron microscopy (HR-TEM) was used to investigate the van der Waals (vdW) gap between the GeTe and Sb_2Te_3 films and the sample microstructure. For comparison of electrical properties between the iPCM samples, 200-nm-thick $Ge_2Sb_2Te_5$ alloy was fabricated by radio-frequency magnetron sputtering. The resistance-voltage (R-V) and conductance values of the iPCM samples were monitored with Keithley 4200A-SCS.

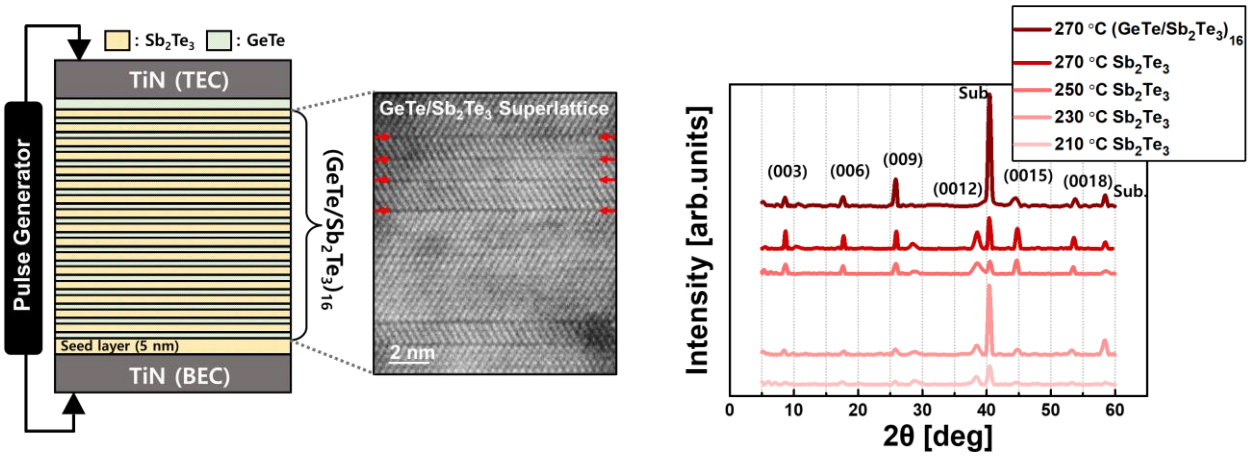

(**a**) (**b**)

Figure 1. (**a**) Schematic of $(GeTe/Sb_2Te_3)_{16}$ iPCM and high-resolution TEM image of a typical $(GeTe/Sb_2Te_3)_n$ material on silicon. The red arrow indicates the vdW gap between the thin films. (**b**) XRD peaks for each (00*l*) plane of the grown Sb_2Te_3 films and $(GeTe/Sb_2Te_3)_{16}$ interfacial materials fabricated with different annealing temperatures.

3. Results and Discussion

The XRD spectra of bulk Sb_2Te_3 and $(GeTe/Sb_2Te_3)_{16}$ iPCMs with growth temperatures ranging from 210 °C to 270 °C are shown Figure 1(b). All observed peaks can be indexed as 00*l* peaks of the Sb_2Te_3, indicating that the fabricated samples possess the preferred orientation, with the c-axis normal to the substrate surface. Increases to the annealing temperature corresponds to crystal growth along the (00*l*) orientation. Figure 1(b) clearly shows that the most highly oriented Sb_2Te_3 film was grown at 270 °C. This result suggests that the thin film with the best quality under different growth conditions can provide a seed layer for the two-step growth method. Therefore, the $(GeTe/Sb_2Te_3)_{16}$ iPCM deposited at an annealing temperature of 270 °C grew to be highly oriented. However, no peaks originating from the GeTe are observed, indicating that the Ge atoms are in different

Preprints (www.preprints.org) | NOT PEER-REVIEWED | Posted: 27 September 2021 doi:10.20944/preprints202109.0444.v1

positions compared to the orientation of the substrate. In addition, it can be seen that the full width at half maximum (FWHM) of the peaks in the (00*l*) direction are broadened in the $(GeTe/Sb_2Te_3)_{16}$ structure. There is a strong possibility that this broadening is caused by Sb_2Te_3 strain due to the Ge atoms moving or intermixing between layers [16].

The resistance-voltage (R-V) curves of the $(GeTe/Sb_2Te_3)_{16}$ iPCM memory cell are shown in Figure 2(a). The pulse programming consists of a 0.05 V rectangular pulses applied to the $(GeTe/Sb_2Te_3)_{16}$ iPCM with a given pulse width (PW). Bidirectional switching is observed, in which the high resistance state (HRS) and the low resistance state (LRS) coexist at one polarity under all ISPP conditions (fixed at 70 ns to 1 μs). We generally refer to the transition from the HRS to the LRS as the SET operation, and the opposite is called the RESET operation. The iPCM mechanism is strongly influenced by the bonding phase of Ge atoms, as mentioned earlier. Covalently bonded Ge atoms in the superlattice-structured iPCM are separated by a crystalline Sb_2Te_3 plane. As shown in the simplified model in Figure 1(a), the distributed Ge atoms in the GeTe layer are switched from a covalently bonded 4-fold structure to a resonantly bonded 6-fold structure by charge injection. DFT calculations confirmed that the 4-fold structure and the 6-fold structure are stable [17,18]. Figure 2(b) shows that as the PW applied to $(GeTe/Sb_2Te_3)_{16}$ iPCM increases, the resistance ratio between HRS and LRS increases, and the window voltage that maintains the LRS decreases. Moreover, the threshold voltage for transitioning from the initial RESET state to the SET state is 0.1 V higher at 70 ns PW than at 1 μs PW. In the case of ISPP with a PW of 1 μs, the resistance ratio, which is the highest HRS value divided by the lowest LRS value, is about 62.2, and the LRS window margin is 0.45 V, as shown in Figure 2(b). On the other hand, when ISPP is applied with the shortest PW of 70ns, a resistance ratio of about 12.6 and a SET margin of 0.95 V is obtained. This result seems to imply that a trade-off exists between the resistance ratio and the window margin of the LRS.

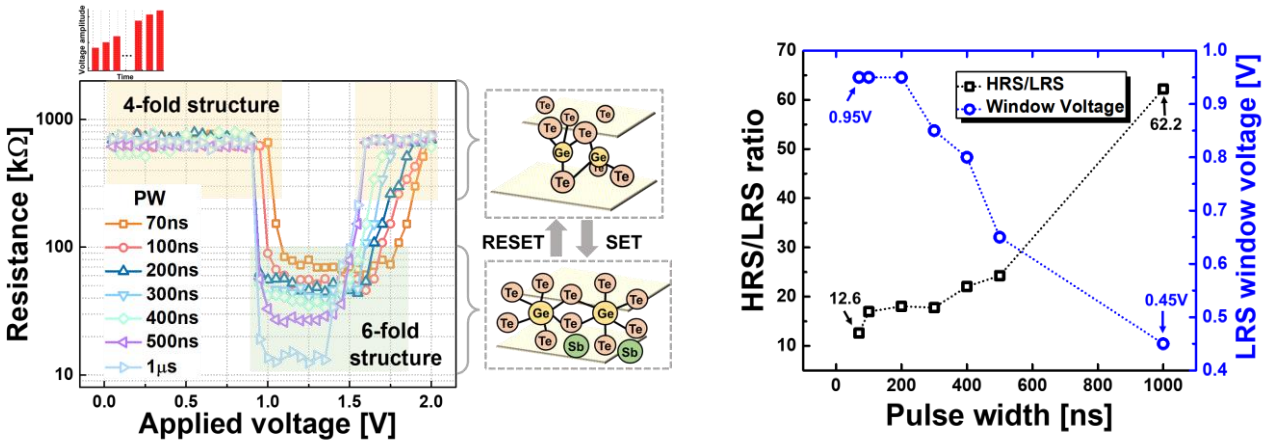

(**a**) (**b**)

Figure 2. (**a**) Reversible resistance switching of the resistance-voltage (R-V) characteristics of the $(GeTe/Sb_2Te_3)_{16}$ iPCM devices for different pulse widths and a schematic of a simplified transition model of the iPCM. (**b**) The HRS/LRS ratio (black) and LRS window voltage (blue) as a function of the applied pulse width.

Interestingly, the R-V characteristics are not as clearly controlled by PW for GST225 alloy as they are for $(GeTe/Sb_2Te_3)_{16}$ iPCMs. This difference is due to the less-ordered GST225 alloy having a broad distribution of transition energies as atomic movement occurs in all directions. Therefore, it is difficult to perform a stable operation using PW in the GST225 alloy compared to in the ideally ordered Ge atoms of the GeTe interface. Moreover, a $(GeTe/Sb_2Te_3)_{16}$ iPCM can be expected to lower the operating voltage due to entropy reduction from the limited atomic movement of Ge atoms located between Sb_2Te_3 layers, which is a hexagonal template in an ideal superlattice nature. In the ideal case, the Ge atoms experience the same force and change to covalent bonding with high resistance from resonant bonding with low resistance when an electric pulse is applied to the GeTe

Preprints (www.preprints.org) | NOT PEER-REVIEWED | Posted: 27 September 2021 doi:10.20944/preprints202109.0444.v1

thin film in the iPCM nanostructure. However, an actual $(GeTe/Sb_2Te_3)_{16}$ iPCM has different switching characteristics depending on the PW condition because the vdW interaction does not apply the same force to all layers and the Ge atoms in the GeTe thin film are not all located at the interface, which is discussed in more detail below. Note that, as shown in Figure 2(a), when the PW is applied to the shortened ISPP, $(GeTe/Sb_2Te_3)_{16}$ iPCMs have the potential for more intermediate states to emerge. This result implies that the $(GeTe/Sb_2Te_3)_{16}$ iPCM has the latent ability to implement gradual LTP/LTD, which is one of the synaptic properties suitable for analog design, according to appropriate electrical pulse programming.

To implement an artificial synaptic device using the iPCM, gradual and symmetric LTP/LTD and multiple conductance values that mimic analog behavior should be achieved by applying electrical pulses. Applying identical pulses of equal intensity places less burden on the circuit than more complex programming schemes, such as varying the voltage amplitude or pulse width. Figure 3 displays the conductance-voltage (C-V) graph when applying the $(GeTe/Sb_2Te_3)_{16}$ iPCM according to the PW and voltage amplitude in the identical scheme. The solid lines in the graph correspond to Boltzmann functions along the conductance values for clearly comparing linearity. An identical pulse scheme with an amplitude of 0.6 V exhibits potentiation properties that increase the conductance values, as shown in Figure 3(a). To initialize the first $(GeTe/Sb_2Te_3)_{16}$ iPCM with high resistance, ISPP with 1 μs PW was applied to achieve the HRS. As the PW of the pulse scheme increases, the conductance achieves higher values. Each PW of a given pulse scheme produces a different maximum conductance value at saturation. When comparing the 70 ns PW to the 1 μs PW, it appears that the 70 ns PW is achieved gradually conductance increased and has more effective conductance states. This characteristic is consistent with the bidirectional switching properties shown above. Therefore, it can be inferred that there is a trade-off between dynamic range and effective conductance states as determined by PW. In addition, this result implies that identical pulse schemes with PW modulation can be used to implement multiple values of conductance or potentiation.

Figure 3(b) shows the conductance values produced by the application of a given pulse scheme with the PW fixed at 70 ns and different voltage amplitudes (1.6 V to 2.2 V) to the $(GeTe/Sb_2Te_3)_{16}$ iPCM. When the amplitude is greater than 1.6 V, the pulses have a depression characteristic, in which conductance decreases. Initialization was set by applying an identical 0.6 V pulse scheme with a 70 ns PW until saturation. It was observed that the effective conductance states were not sufficiently implemented in the identical pulse scheme with a voltage amplitude of 2.2 V because the conductance value drops abruptly at this voltage. In the case of the identical pulse scheme at 1.4 V, the conductance decreases too gradually, making it difficult to distinguish varying conductance values. Therefore, considering the possible conductance states and the dynamic range, it is reasonable to suppose that the identical pulse scheme with an amplitude of 1.8 V is suitable for a depression pulse. The evidence suggests that if voltage amplitude and conductance values are precisely controlled, not only gradual conductance increased or decreased properties but also high symmetry between potentiation and depression can be realized.

As illustrated by Figure 4(a), we modeled the $GeTe/Sb_2Te_3$ iPCM to discuss how it can implement multiple conductance states. When the phase transition in the superlattice structure is considered as an equivalent circuit model, it can be viewed as a partial and parallel model. In the parallel model, the GeTe layers shift one by one, and in the series structure, the phase transition occurs partially in the entire layer. Since more conductance states are found than the number of GeTe layers, it seems that the $GeTe/Sb_2Te_3$ iPCM is better described by the partial structure model than the parallel structure. This result is consistent with those for devices with $TiTe_2/Sb_2Te_3$ superlattice structures [19]. Furthermore, the partial transition region restricts structural relaxation by the nanosized effect. It can be assumed that this effect can prevent the conductance variation critical to synapse operation that occurs in GST225 alloy. Indeed, the Te-Te antibonding interaction between the thin films and the Sb_2Te_3 bonding pairs interfere with the enhancement of the Peierls distortion [20]. Therefore, as shown in partial model 1 of Figure 4(a), an identical pulse

Preprints (www.preprints.org) | NOT PEER-REVIEWED | Posted: 27 September 2021 doi:10.20944/preprints202109.0444.v1

scheme with short PW or low voltage amplitude is proportional to the amount of energy applied to the iPCM, implying a relatively small area of transition.

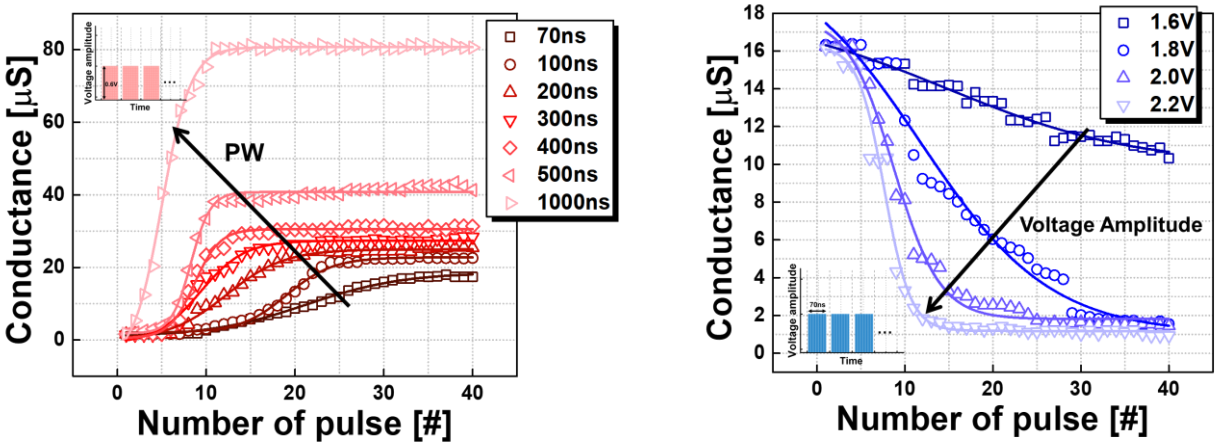

(**a**) (**b**)

Figure 3. Potentiation and depression characteristics of the $(GeTe/Sb_2Te_3)_{16}$ iPCM with identical pulses. (**a**) Potentiation characteristics of pulses fixed at 0.6 V with different PWs. (**b**) Depression characteristics for pulses fixed at 70 ns with different voltage amplitudes.

As the PW, voltage amplitude or the number of applied pulses increases, the partial area becomes wider and saturated due to an avalanche of Ge atomic switching caused by biaxial strain [21]. This result is reasonable in that there are studies that show a temperature distribution resulting from the application of an external stimulus to a superlattice device. Figure 4(b) schematically describes the interatomic potential for Ge atomic switching for partial 1, 2 and 3. In partial 1, Ge atoms are in a region that requires a low activation energy for diffusive atomic switching, which could be represented by a short PW. In this situation, more Ge atoms have to cross a larger energy barrier to flip through the Te plane. Therefore, it can be inferred that the switching process of the iPCM has a linear dependence with multiple conductance states. It can be inferred that partial 1 can be controlled more precisely when a short PW is applied. Evolution from partial 1 to partial 2 or right to partial 3 occurs when a continuous pulse train is applied to partial 1. On the other hand, there is a strong possibility that partial 1 and 2 will be skipped and a sharp transition will occur when sufficient activation energy is applied to cross the energy barrier. However, in actual Ge atomic movement near the vdW gap, there is an additional lateral process or a complex switching process that includes intermixing with the Sb_2Te_3 layer.

On the basis of the observed analog behavior driven by the iPCM systems, we evaluated the synaptic weight cumulative characteristics by applying optimized pulses, as shown in Figure 5. In addition, comparing Figure 5(a) to Figure 5(b), (c), (d) shows the disparity in the characteristics of artificial synapses that employ GST225 alloy and $(GeTe/Sb_2Te_3)_{16}$ iPCM. Figure 5(a) illustrates a pulse programming design that differentiates between potentiation pulses and depression pulses for GST225 alloy using the melt-quenching mechanism. Application of this pulse scheme results in appropriate electrical excitation for controlling the amorphous and crystalline states in the active region. For potentiation, a pulse scheme decreasing by 0.05 V steps from 2 V to 0.5 V and using 3 μs PWs was applied for joule annealing. In contrast, the depression pulse scheme increased from 2.5 V to 4 V using 70 ns PWs to accomplish melting of materials in the crystalline state. As shown in Figure 5(a), gradual potentiation and depression with 30 conductance states were realized in the GST225 alloy by applying stair-case pulses. However, it is well-known that mushroom-shape PCRAM devices usually change resistance abruptly to achieve amorphization and crystallization. The GST225 alloy samples also resulted in undesirable weight-update asymmetry in synaptic potentiation and depression (marked with a brown circle drawn in Figure 5(a)). In the case of the $(GeTe/Sb_2Te_3)_{16}$ iPCM, the

Preprints (www.preprints.org) | NOT PEER-REVIEWED | Posted: 27 September 2021 doi:10.20944/preprints202109.0444.v1

most gradual synaptic weight cumulative condition was implemented. It is reasonable to suppose that the voltage amplitudes for the depression pulse and the potentiation pulse should be 0.6 V and 1.8 V, respectively. Although the appropriate voltage amplitude could be changed by varying the PW, the synaptic characteristic can also be implemented by fixing the pulse width. As ca be observed in Figure 5(b), (c), (d), all PW conditions (70 ns, 300 ns, 1μs) achieved potentiation and depression by applying the identical pulse scheme.

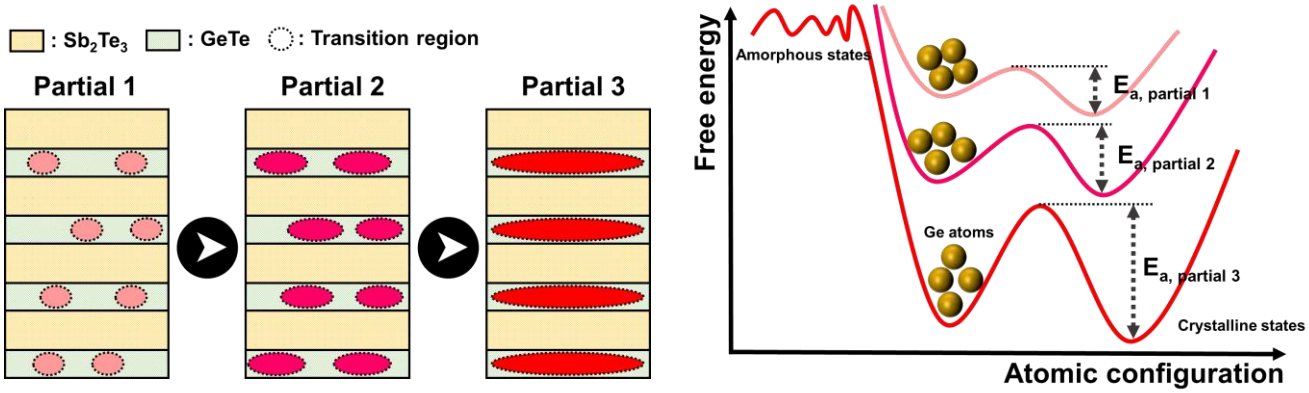

(**a**) (**b**)

Figure 4. (**a**) Partial model of the GeTe/Sb_2Te_3 iPCM. (**b**) The schematic interaction potential for Ge atomic switching in a GeTe/Sb_2Te_3 iPCM.

To compare synaptic characteristics, the nonlinearity (NL) of the GST225 alloy and the $(GeTe/Sb_2Te_3)_{16}$ iPCM was calculated for the applied pulse programming schemes. NL was adopted to effectively analyze the LTP and LTD phenomena, which are characteristics of a bio-synapse. The calculation was derived using equation (1). $G_P(n)$ and $G_D(n)$ are the conductance values after the nth potentiation pulse and depression pulse, and N is the number of potentiation pulses/depression pulses. Table 1 shows the results of the NL values calculated using equation (1). The GST225 alloy showed a relatively large NL value of 0.58 due to the abrupt change in conductance during phase transition between the amorphous and crystalline states. In the case of the $(GeTe/Sb_2Te_3)_{16}$ iPCM, as the PW shortened from 1 μs to 70 ns, lower values of NL are indicated. This result implies that applying sufficient energy helps exceed the activation energy barrier for the transition of the Ge atom saturated under the relatively long PW condition of 1 μs, in accordance with the partial model mentioned above. Therefore, under the condition of the shortest PW of 70 ns, the conductance values of LTP and LTD were more precisely controlled, as indicated by a NL of 0.32. Furthermore, PW is also related to the number of conductance states of LTP/LTD. In the identical pulse scheme with 70 ns PWs, 80 conductance states are implemented; demonstrating sophisticated conductance modulation. In contrast, 300 ns and 1 μs PWs could not generate sufficient effective conductance states for operation as synaptic devices.

$$\mathrm{NL} = \mathrm{Max}|G_P(n) - G_D(n)|, n = 1, 2, 3, \ldots, \mathrm{N} \quad (1)$$

However, the dynamic range for measuring the ratio of the largest conductance values to the smallest conductance values is 13.1 with 70 ns PW, whereas GST225 has the largest observed dynamic range of 90.2. As shown in Table 1, the potentiation pulse scheme using 0.6 V and 70 ns PWs and the depression pulse scheme using 1.8 V and 70 ns PWs achieved the lowest NL value of 0.32. In addition, the number of conductance states achieved with these schemes implemented synaptic characteristics superior to those of other conditions through 40 multiple levels of potentiation and depression. Although the conductance ratio has a narrow range, it is shown that a $(GeTe/Sb_2Te_3)_{16}$ iPCM can achieve linear and symmetric LTP/LTD in identical pulse systems.

Preprints (www.preprints.org) | NOT PEER-REVIEWED | Posted: 27 September 2021 doi:10.20944/preprints202109.0444.v1

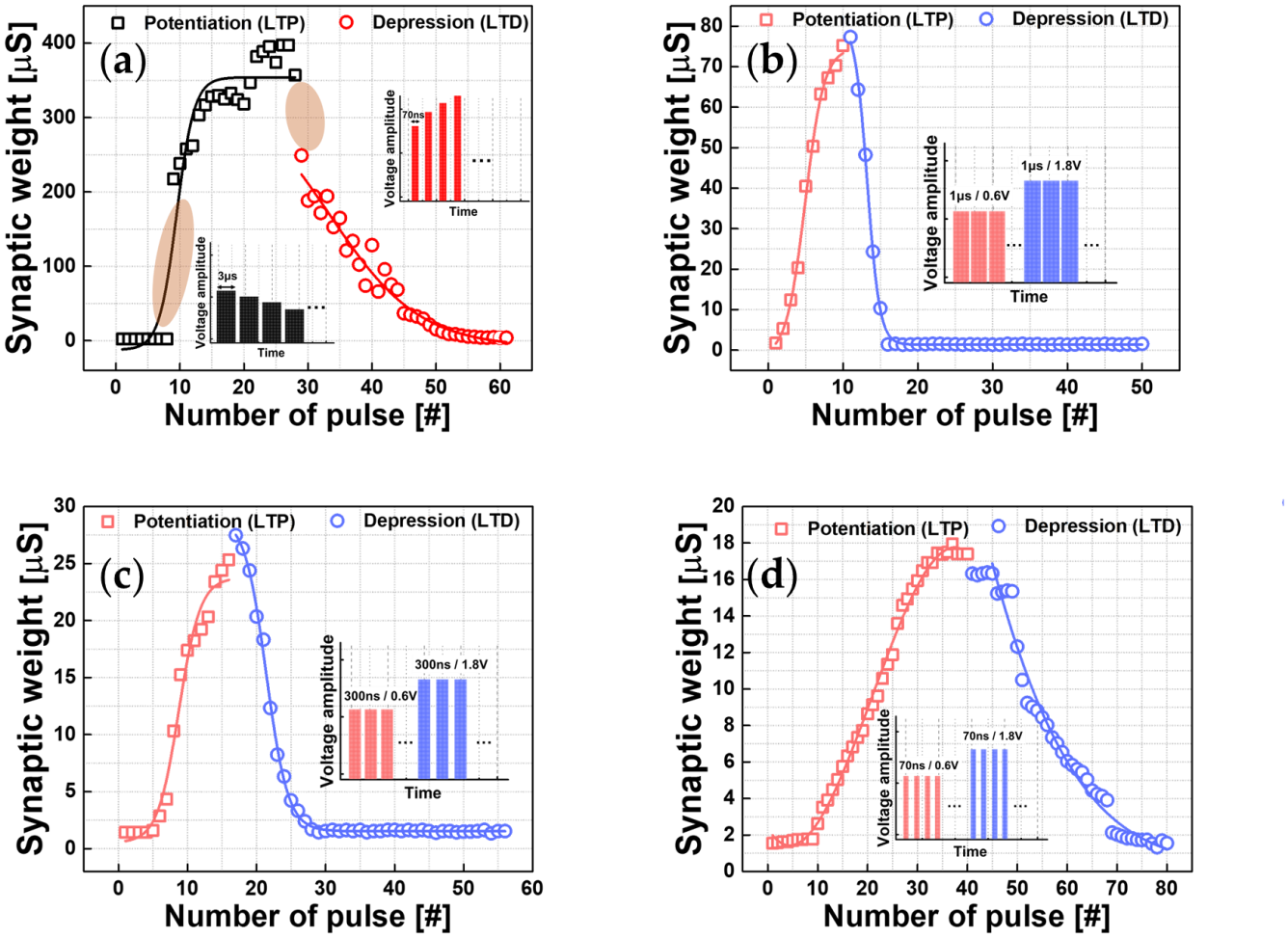

Figure 5. Conductance modulation curves obtained in GST225 alloy and $(GeTe/Sb_2Te_3)_{16}$ iPCM devices. (**a**) Long-term potentiation (LTP) and long-term depression (LTD) of GST225 alloy, the pulse scheme of the pulse train applied for LTP and LTD (inset). (The brown circles indicate the ranges in which conductance values change abruptly.) LTP/LTD obtained by applying an identical pulse scheme to a $(GeTe/Sb_2Te_3)_{16}$ iPCM with (**b**) a potentiation pulse of 1 μs PW and 0.6 V and a depression pulse of 1 μs PW and 1.8 V, (**c**) a potentiation pulse of 300 ns PW and 0.6 V and depression pulse of 300 ns PW and 1.8 V and (**d**) a potentiation pulse of 70 ns PW and 0.6 V and a depression pulse of 70 ns and 1.8 V.

Table 2. Summary of synaptic characteristics of GST225 alloy and $(GeTe/Sb_2Te_3)_{16}$ iPCM.

	NL	Effective conductance states (LTP/LTD)	Dynamic range (G_{max}/G_{min})
(a) GST225 alloy	0.58	30/30	90.2
(b) $(GT/ST)_{16}$ iPCM (PW 1μs)	0.54	10/10	58.0
(c) $(GT/ST)_{16}$ iPCM (PW 300Ns)	0.41	16/16	19.2
(d) $(GT/ST)_{16}$ iPCM (PW 70ns)	0.32	40/40	13.1

4. Conclusions

In this paper, we introduced a solution for an artificial bidirectional synapse using $GeTe/Sb_2Te_3$ with a superlattice structure based on interfacial phase change memory. Based on the bidirectional switching characteristics, we demonstrated the realization of a gradual resistance change through the relationship between PW and resistance. The $(GeTe/Sb_2Te_3)_{16}$ iPCM using the designed identical pulse scheme conditions with optimized voltage amplitude and PW achieved potentiation and depression based on the

finely controlled partial model of Ge atomic movement in the superlattice. Therefore, the $(GeTe/Sb_2Te_3)_{16}$ iPCM achieved 0.32 NL and 80 conductance states when a potentiation pulse (0.6 V, 70 ns PW) and a depression pulse (1.8 V, 70 ns PW) were applied. This gradual/symmetric conductance modulation characteristic is expected to be superior to GST 225, with 0.58 NL, when applied to artificial synapses. Therefore, the $(GeTe/Sb_2Te_3)_{16}$ iPCM with a vdW gap structure has demonstrated potential as a useful device for artificial memory with linear LTP/LTD. In this regard, the tuning of the gradual and symmetric conductance changes of $GeTe/Sb_2Te_3$ iPCMs using voltage-based identical pulse schemes could be applied to artificial synaptic devices in a hardware neural network with high performance.

Author Contributions: For research articles with several authors, a short paragraph specifying their individual contributions must be provided. The following statements should be used "Conceptualization, Shin-young Kang and Ju-young Lee.; methodology, Soo-min Jin and Dae-seong Woo.; validation, Yun-heub Song and In-ho Nam and Z.Z.; formal analysis, Shin-young Kang.; investigation, Shin-young Kang, Soo-min Jin; resources, Tae-hun Shim.; data curation, Yun-heub Song.; writing—original draft preparation, Shin-young Kang.; writing—review and editing, Yun-heub Song, Yuji Sutou, Jae-gun Park.; visualization, Shin-young Kang and Soo-min Jin.; supervision, Yun-heub Song, Yuji Sutou, Jae-gun Park.; All authors have read and agreed to the published version of the manuscript.

Funding: This research was supported by the MOTIE (Ministry of Trade, Industry & Energy) (project number 10080625) and KSRC (Korea Semiconductor Research Consortium) support program for the development of the future semiconductor device.

Conflicts of Interest: The authors declare no conflict of interest. The funders had no role in the design of the study; in the collection, analyses, or interpretation of data; in the writing of the manuscript, or in the decision to publish the results.

References

1. Xi, Yue, et al. In-memory learning with analog resistive switching memory: A review and perspective. *Proceedings of the IEEE*, **2020**, *109.1*, 14-42.
2. Islam, R.; Li, H.; Chen, P.Y.; Wan, W.; Chen, H.Y.; Gao, B.; Wu, H.; Yu, S.; Saraswat, K.; Wong, H.P. Device and materials requirements for neuromorphic computing. *Journal of Physics D: Applied Physics* **2019**, *52*, 113001.
3. LeCun, Y.; Bengio, Y.; Hinton, G. Deep learning. nature 521 (7553), 436-444. *Google Scholar Google Scholar Cross Ref Cross Ref* **2015.**
4. Horowitz, M. 1.1 computing's energy problem (and what we can do about it). *2014 IEEE International Solid-State Circuits Conference Digest of Technical Papers (ISSCC)*, **2014**, pp. 10–14.
5. Song, K.M.; Jeong, J.S.; Pan, B.; Zhang, X.; Xia, J.; Cha, S.; Park, T.E.; Kim, K.; Finizio, S.; Raabe, J. Skyrmion-based artificial synapses for neuromorphic computing. *Nature Electronics* **2020**, *3*, 148–155.
6. Seo, S.; Kang, B.S.; Lee, J.J.; Ryu, H.J.; Kim, S.; Kim, H.; Oh, S.; Shim, J.; Heo, K.; Oh, S. Artificial van der Waals hybrid synapse and its application to acoustic pattern recognition. *Nature communications* **2020**, *11*, 1–9.
7. Yu, S.; Wu, Y.; Jeyasingh, R.; Kuzum, D.; Wong, H.S.P. An electronic synapse device based on metal oxide resistive switching memory for neuromorphic computation. *IEEE Transactions on Electron Devices* **2011**, *58*, 2729–2737.
8. Jerry, M.; Chen, P.Y.; Zhang, J.; Sharma, P.; Ni, K.; Yu, S.; Datta, S. Ferroelectric FET analog synapse for acceleration of deep neural network training. 2017 IEEE International Electron Devices Meeting (IEDM), 2017, pp. 6–2.
9. Kuzum, D.; Jeyasingh, R.G.; Lee, B.; Wong, H.S.P. Nanoelectronic programmable synapses based on phase change materials for brain-inspired computing. *Nano letters* **2012**, *12*, 2179–2186.
10. Gallo, M.L.; Sebastian, A. An overview of phase-change memory device physics. *Journal of Physics D: Applied Physics* **2020**, *53*, 213002.
11. Wong, H.S.P.; Raoux, S.; Kim, S.; Liang, J.; Reifenberg, J.P.; Rajendran, B.; Asheghi, M.; Goodson, K.E. Phase change memory. *Proceedings of the IEEE* **2010**, *98*, 2201–2227.
12. Bichler, O.; Suri, M.; Querlioz, D.; Vuillaume, D.; DeSalvo, B.; Gamrat, C. Visual pattern extraction using energy-efficient "2- PCM synapse" neuromorphic architecture. *IEEE Transactions on Electron Devices* **2012**, *59*, 2206–2214.
13. Simpson, R.E.; Fons, P.; Kolobov, A.V.; Fukaya, T.; Krbal, M.; Yagi, T.; Tominaga, J. Interfacial phase-change memory. *Nature nanotechnology* **2011**, *6*, 501–505.
14. Yu, X.; Robertson, J. Modeling of switching mechanism in GeSbTe chalcogenide superlattices. *Scientific reports* **2015**, *5*, 1–8.
15. Kolobov, A.V.; Fons, P.; Saito, Y.; Tominaga, J. Atomic reconfiguration of van der Waals gaps as the key to switching in GeTe/Sb2Te3 superlattices. *ACS omega* **2017**, *2*, 6223–6232.

16. Saito, Y.; Fons, P.; Kolobov, A.V.; Mitrofanov, K.V.; Makino, K.; Tominaga, J.; Hatayama, S.; Sutou, Y.; Hase, M.; Robertson, J. High-quality sputter-grown layered chalcogenide films for phase change memory applications and beyond. *Journal of Physics D: Applied Physics* **2020**, *53*, 284002.
17. Tominaga, J.; Shima, T.; Fons, P.; Simpson, R.; Kuwahara, M.; Kolobov, A. What is the origin of activation energy in phase-change film? *Japanese journal of applied physics* **2009**, *48*, 03–053.
18. Soeya, S.; Shintani, T. Crystalline structure of GeTe layer in GeTe/Sb2Te3 superlattice for phase change memory. *Journal of Applied Physics* **2012**, *112*, 034301.
19. Ding, K.; Wang, J.; Zhou, Y.; Tian, H.; Lu, L.; Mazzarello, R.; Jia, C.; Zhang, W.; Rao, F.; Ma, E. Phase-change heterostructure enables ultralow noise and drift for memory operation. *Science* **2019**, *366*, 210–215.
20. Hu, Y.C.; Li, Y.W.; Yang, Y.; Guan, P.F.; Bai, H.Y.; Wang, W.H. Configuration correlation governs slow dynamics of supercooled metallic liquids. *Proceedings of the National Academy of Sciences* **2018**, *115*, 6375–6380.
21. Zhou, X.; Behera, J.K.; Lv, S.; Wu, L.; Song, Z.; Simpson, R.E. Avalanche atomic switching in strain engineered Sb2Te3-GeTe interfacial phase-change memory cells. *Nano Futures* **2017**, *1*, 025003.